

Diffuse Ultraviolet Sky Toward Nearby Galaxy Clusters

K. M. Minu^{1,2}, N. V. Sujatha¹, and K. F. Fency^{1,3}

Department of Physics, St. Xavier's College for Women, Aluva 683101, India; minu@sncollegenattika.ac.in, sujathanv@stxaviersaluva.ac.in, fencykf@sacredheartcollege.ac.in

Department of Physics, Sree Narayana College, Nattika 680566, India

Department of Physics, Stee Narayana Conege, Natura 080300, India

3 Department of Physics, Sacred Heart College, Chalakudy 680307, India

Received 2025 May 10; revised 2025 July 30; accepted 2025 September 10; published 2025 October 16

Abstract

This study examines diffuse ultraviolet (UV) emissions in the PHOENIX_00 region near galaxy clusters using GALEX deep observations. In the far-UV (FUV) and near-UV (NUV), we detected backgrounds of 125–200 and 225–350 photon units (PU), with scatters of ± 16 and ± 22 PU, respectively. A moderate FUV-NUV correlation and FUV/NUV ratio below unity indicate FUV-dominated emission and little molecular hydrogen fluorescence or hot-line contributions. Dust influences the FUV background more strongly than the NUV, and UV band emissions correlate more strongly at Galactic latitudes $|gb| > 71\,^{\circ}$. 29. Infrared (IR) color ratios IR_{60}/IR_{100} ($\approx 0.34 \pm 0.03$) indicate homogeneous large-grain temperatures and depletion of small grains and PAHs, while IR_{60}/IR_{25} below 3 indicates AGN activity in the region. The non-zero offsets of IR-UV plots 89 PU (FUV) and 199 PU (NUV) indicate the region's baseline illumination and extragalactic radiation. Approximately 11% of the FUV offset and 23% of the NUV offset come from extragalactic background light, while the rest comes from dust-scattered starlight. Finally, our research shows that the interstellar radiation field directly affects the UV background, with the strength inversely proportional to local dust content.

Key words: ultraviolet: ISM - scattering - (ISM:) dust, extinction - infrared: ISM

1. Introduction

Interstellar dust accounts for a small fraction of the universe's mass, yet plays a critical role in generating the diffuse ultraviolet (UV) background radiation. This faint glow serves as an important, though not fully understood, marker of astrophysical processes-from dust scattering to the large-scale events driving cosmic reionization. Analyzing the composition of diffuse UV galactic light sheds light on the dynamics of the interstellar medium (ISM), including factors such as line emissions, molecular hydrogen fluorescence, and dust grain scattering, as well as the influence of extragalactic light. In recent times, many studies have improved our knowledge of the ISM's structure, dynamics, and physical properties (Cox 2005).

The diffuse UV background provides valuable insight into the broader structure and evolution of the cosmos by revealing key characteristics of both the ISM and the intergalactic medium (IGM). In the diffuse ISM, dust-scattered radiation is the dominant component from UV to near-infrared (near-IR) (\sim 0.2–2 μ m) (Bowyer 1991; Murthy et al. 2010), while thermal emission from very small grains and large molecules, such as polycyclic aromatic hydrocarbons (PAHs), heated by the interstellar radiation field (ISRF), dominates from near-IR to mid-infrared (mid-IR) (\sim 2–50 μ m). However, challenges persist due to complex foreground emissions, uncertainties in dust reflectivity, and the need for precise calibration.

Narayanan et al. (2023a, 2023b) recently created and tested an empirical model of foreground emission in UV using the Galaxy Evolution Explorer (GALEX) deep observations. This model predicts airglow emission, which is a major foreground in UV observations, based on 10.7 cm solar flux and Sun angle. The model splits the total airglow into a constant part (AGc) and a varying part (AGv). It predicts values between 85 and 390 photons cm⁻² s⁻¹ sr⁻¹ \mathring{A}^{-1} (photon units, PU) in the far-ultraviolet (FUV) and between 80 and 465 PU in the nearultraviolet (NUV) using GALEX deep observations. However, a notable non-scattered component has been observed in low column density regions near the Galactic poles (Henry 1991; Hamden et al. 2013; Murthy 2016). Zhitnitsky (2022) suggested that dark matter annihilation within the Axion Quark Nugget framework could be a possible source of the diffuse UV background.

Galaxy clusters are the largest gravitationally bound structures in the universe, which include gas and a significant amount of dark matter in addition to galaxies. The distribution of dark matter, gas, and stars within them has been better understood by recent observations made at various wavelengths, from microwaves to X-rays (Burchett et al. 2019). Welch et al. (2020) suggest that galaxy clusters play a role in generating the diffuse extragalactic background, with a flux of approximately 12 ± 2 PU in the FUV range. Their findings provide strong evidence that the majority of this contribution

Table 1
Observation Log

Tile Name	PHOENIX_00
gl	293 [°] .76
gb	-71.25
NUV Exposure	13213.6 s
FUV Exposure	7966.5 s
NUV Visits	12
FUV Visits	8

comes mainly from non-thermal emission processes and intracluster light. Recent studies have shown that the relationship between UV and infrared (IR) radiation is particularly significant in galaxy clusters (Bordoloi et al. 2024). This connection helps in determining the temperature and nature of dust grains.

This study focuses on the PHOENIX_00 target, situated near the South Galactic Pole (SGP) at a high latitude (gb: -71.25) and a longitude (gl) of 293.76. This target was chosen to estimate the upper limit of the contribution of unresolved extragalactic background light (EGL) in the diffuse UV background due to its unique nature of high Galactic latitude, low optical depth, and large concentration of galaxy clusters and groups. GALEX Deep Imaging Survey (DIS) only covered a few cluster-rich locations; thus, the PHOENIX_00 target is a unique and excellent opportunity to assess the EGL contribution, improving our understanding of diffuse UV light at high latitudes. The SIMBAD Astronomical Database (Wenger et al. 2000) lists 72 galaxy clusters and seven galaxy groupings within one degree of PHOENIX 00. Among these, the GALEX survey identified five galaxies within a 0.625 radius, including clusters and groups such as IC 1633, ESO 243-41, ESO 243-45, ESO 243-51 and ESO 243-52 (Gil de Paz et al. 2007). To explore this region, we utilized GR6/GR7 DISs from GALEX, the SIMBAD database and the Wide-field Infrared Survey Explorer (WISE) active galactic nucleus (AGN) catalog toward the target. GALEX made eight deep FUV and 12 NUV observations toward the target, with a total exposure time of 2.22 and 3.67 hr, respectively. Detailed observation logs and target information are provided in Tables 1 and 2.

2. Observations and Data Analysis

The GALEX probe was launched into space by NASA's Small Explorer (SMEX) program in 2003. The main scientific goal of the GALEX spacecraft was to map the history and distribution of star formation in the universe over the past 10 billion years (Martin et al. 2005). A single 50 cm telescope collects light from the sky and uses microchannel plate detectors to get clear pictures in the NUV (1750–2850 Å) and FUV (1350–1750 Å) ranges. A dichroic mirror and a grism are used for low-resolution spectroscopy. GALEX provides

coverage over a 1 $^{\circ}$.25 field of view in the sky and offers an effective spatial resolution of 5''-7''. The telescope collected data as time-tagged photon events, observing about 77% of the sky at various depths in at least one band. After the primary mission ended, an extension called CAUSE was run by Caltech, which observed bright regions that were not visited long enough for science.

In this study, we used the intensity maps of the region from both FUV and NUV bands in the form of Flexible Image Transport System (FITS; Wells et al. 1981) files and the GALEX pipeline (Morrissey et al. 2007) generated catalog of point sources, with flux measurements from source extractor (SExtractor; Bertin & Arnouts 1996). Most of the radiation observed by GALEX comprises diffuse radiation, which is further separated into foreground and background radiations. Less than 7% of the signal comes from point sources (Sujatha et al. 2009). We extracted diffuse UV maps of the PHOE-NIX 00 region in FUV and NUV by removing point sources listed in the GALEX merged catalog from the corresponding intensity images and re-binning the images to 4' resolution (160 × 160 GALEX pixels) to enhance the signal-to-noise ratio as described by Sujatha et al. (2009, 2010). We analyzed the diffuse UV maps of the PHOENIX 00 region to examine its characteristics, focusing on the inner 1.1 diameter to eliminate edge effects. In addition to the instrumental dark count, the data may encompass background radiations, including dust-scattered starlight, atomic and molecular emissions, as well as extragalactic radiation, in addition to the foreground radiations such as airglow and zodiacal light.

As per Morrissey et al. (2007), the instrumental dark count in each band is estimated to be less than 5 PU. Using the foreground emission model of Narayanan et al. (2023a), the undesirable foreground radiation, airglow, for the region is estimated and removed. To further refine the data, the zodiacal light, corresponding to the ecliptic coordinates of the target and Sun, is also estimated and removed using the lookup table made by Sujatha et al. (2009) based on Leinert et al. (1998) (Table 3). We extract the true astrophysical sky background for the region under study after eliminating these foreground contributions.

We used the intensity of IR $100\,\mu\mathrm{m}$ from the SFD map (Schlegel et al. 1998), which combines the Cosmic Background Explorer/Diffuse Infrared Background Experiment (COBE/DIRBE) and Infrared Astronomical Satellite (IRAS) Sky Survey Atlas maps after eliminating point sources and zodiacal signals, as a measure of interstellar dust along the line of sight. In Figure 1, the GALEX field of view of the target is overlaid on the SFD map of the region, showing the variation in dust throughout the region. After subtracting the point sources and foreground contributions from the GALEX observations, diffuse UV background maps of the PHOENIX_00 region were produced. These include emissions from extragalactic and

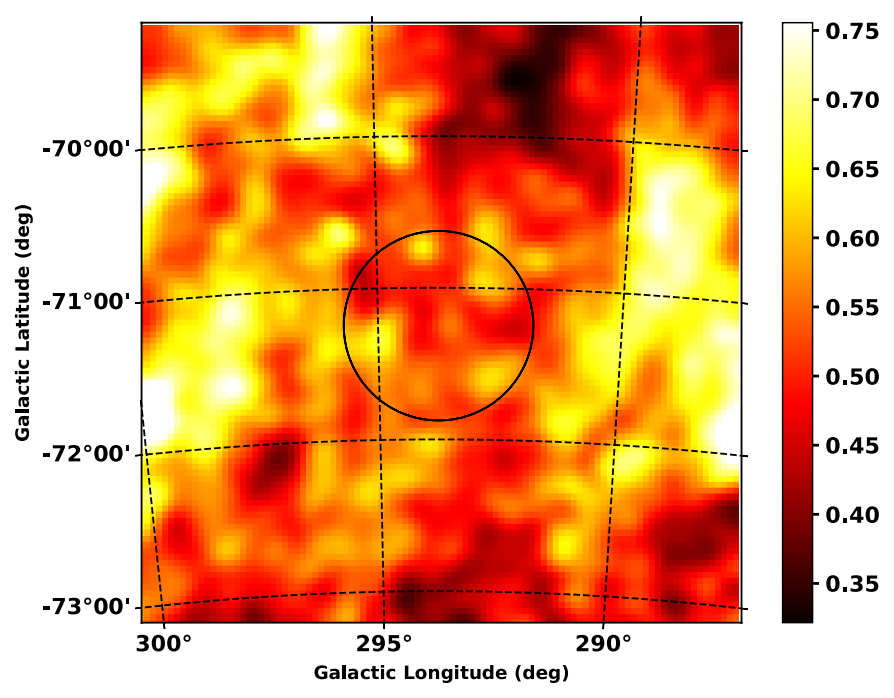


Figure 1. The GALEX field of view of the PHOENIX_00 target is overplotted as a circle on the SFD map of the region.

Table 2
PHOENIX_00: Location Details

Parameters	Range	References	
E(B-V)	0.01–0.02 mag	Planck Collaboration et al. (2014)	
IR $100 \mu m$	$0.42 - 0.63 \mathrm{MJy \ sr^{-1}}$	Schlegel et al. (1998)	
Optical depth, τ	0.09-0.15	Bohlin et al. (1978); Draine (2003)	
$N(H_{\rm I})$	$(1.12-3.46) \times 10^{20} \mathrm{cm}^{-2}$	HI4PI Collaboration et al. (2016)	
${ m H}_{lpha}$	0.1–0.7 R	Finkbeiner (2003)	

Table 3
Foreground Contributions in the Diffuse Map

Foreground Radiations		
(photons cm ⁻² s ⁻¹ sr ⁻¹ \mathring{A}^{-1})		
Instrumental Dark Count	5	
FUV Airglow	261	
NUV Airglow	240	
Zodiacal Light (NUV)	479	

galactic sources, as well as foreground airglow from Earth's atmosphere, among others. Interstellar dust scatters starlight, which makes up the majority of the Galactic portion. H_{II} two-photon emission, line emissions from heated gas, and molecular hydrogen fluorescence also make small contributions. However, feeble IGM emissions contribute very little to the extragalactic portion, which is primarily composed of UV radiation from visible sources, such as galaxies.

 ${\rm H}\alpha$ emission at 656.281 nm shows the existence of ionized hydrogen (H_{II}), a key tracer of star-forming areas and AGNs, where hot, young stars' UV light ionizes surrounding gas. ${\rm H}\alpha$ radiation is widespread in emission nebulae and galaxies, especially in active star formation regions. The rate of star formation in a galaxy or region can be estimated using ${\rm H}\alpha$ emission intensity. ${\rm H}\alpha$ emissions from the region are obtained from the integration of data from the Virginia Tech Spectral-Line Survey (VTSS) in the northern hemisphere and the Southern H-Alpha Sky Survey Atlas (SHASSA; Finkbeiner 2003) in the southern hemisphere. Due to the potential existence of ionized gas or plasma in the PHOENIX_00 region, an ${\rm H}\alpha$ emission has been observed in the range of 0.1–0.7 R. However, no notable relation between the diffuse UV background and ${\rm H}\alpha$ intensity was seen in the region.

The Galactic neutral hydrogen column density ($N(H_I)$) for the specified location is obtained from the H_I 4PI survey 21 cm allsky database (HI4PI Collaboration et al. 2016). $N(H_I)$ observations from the Galactic All-Sky Survey (GASS), which uses the

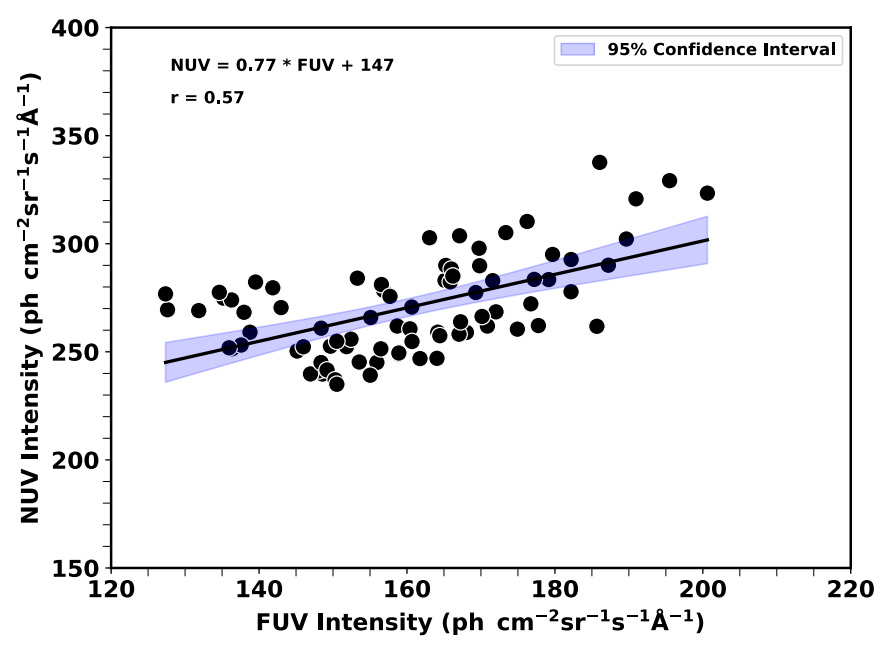


Figure 2. FUV vs. NUV intensities in the PHOENIX_00 region, showing a moderate positive correlation (r = 0.57). The linear fit with 95% confidence interval (shaded) suggests a common origin, likely interstellar dust, despite a scatter of about 20 PU.

Parkes 64 m dish in Australia, and the Effelsberg-Bonn H I Survey (EBHIS), which uses the 100 m radio telescope in Germany, are combined in this database. Using information from the IRAS Improved Reprocessing of the IRAS Survey (IRIS; Miville-Deschênes & Lagache 2005) and the AKARI satellite telescope (Murakami et al. 2007), we have compared diffuse UV radiation with IR emissions at different wavelengths. AKARI provided IR emissions at 90, 140, and 160 μ m, whereas IRIS provided the emissions at 12, 25, 60, and 100 μ m.

3. Results and Discussion

We conducted various correlation analyses to explore the nature and origins of diffuse UV radiation within the PHOENIX_00 region. We specifically looked at the relationship between diffuse UV radiation and IR 100 μ m emission, which provided us with significant information about the properties of diffuse radiation. Each data point in the scatter plots represents the diffuse UV emission at a specific line of sight within the region. Figure 2 shows a moderate positive correlation between the intensity of FUV and NUV in the region, with a Pearson correlation coefficient of r = 0.57. The linear relationship of best fit, NUV = 0.77 FUV + 147, indicates that NUV scales positively with FUV with slope 0.77, which is in good agreement with the previous prediction of Sujatha et al. (2010), although there remains a significant offset. In Figure 3, the ratio of the FUV to NUV intensities is plotted against the intensity of the FUV. A stronger correlation = 0.63) is observed, described by the relation $\frac{\text{FUV}}{\text{NUV}} = 0.002 \text{ FUV} + 0.27$, indicating that at higher FUV intensities, FUV emission dominates NUV emission. Figure 4 represents the FUV/NUV intensity ratio versus the IR $_{100}\,\mu$ m intensity. The moderate correlation (r=0.45) and the relation $\frac{\rm FUV}{\rm NUV}=0.44$ IR $_{100}+0.36$ imply that dust emission, traced by the $100\,\mu$ m band, may help in shaping the observed UV ratio. However, the FUV/NUV ratio in the region is less than unity, indicating the absence of supplementary contributions in the FUV background from other sources, such as hot line emissions, H $_2$ fluorescence, etc. In conclusion, these results highlight the interaction between UV intensities and dust-related processes, with the intensity of FUV appearing to exert a stronger influence on the FUV/NUV ratio than the intensity of NUV alone.

In Figure 5, the diffuse intensities of FUV and NUV are plotted against the 100 μ m IR emissions. A moderate correlation is found between FUV and IR_{100} (r = 0.50, FUV = 155.78 $IR_{100} + 80$), while NUV shows a weaker correlation (r = 0.14, NUV = 57.63 $IR_{100} + 241$). This finding contrasts with our initial expectation of a strong correlation between the IR₁₀₀ and UV intensities, plausibly due to the lack of dust variation and scatter of about 20 PU in the GALEX data. Typically, UV radiation that is not scattered is absorbed by dust, which then increases the dust temperature, leading to re-emission as the IR 100 μ m intensity. The above findings suggest that dust-associated processes traced by 100 μ m emissions more strongly affect the FUV background than the NUV background. The IR emission generally decreases with increasing latitude, reflecting lower dust column densities away from the Galactic plane. Figure 6 represents the variation of IR₁₀₀ emission with Galactic latitudes, and it is evident that the IR emission, which serves as an indicator of dust, remains relatively

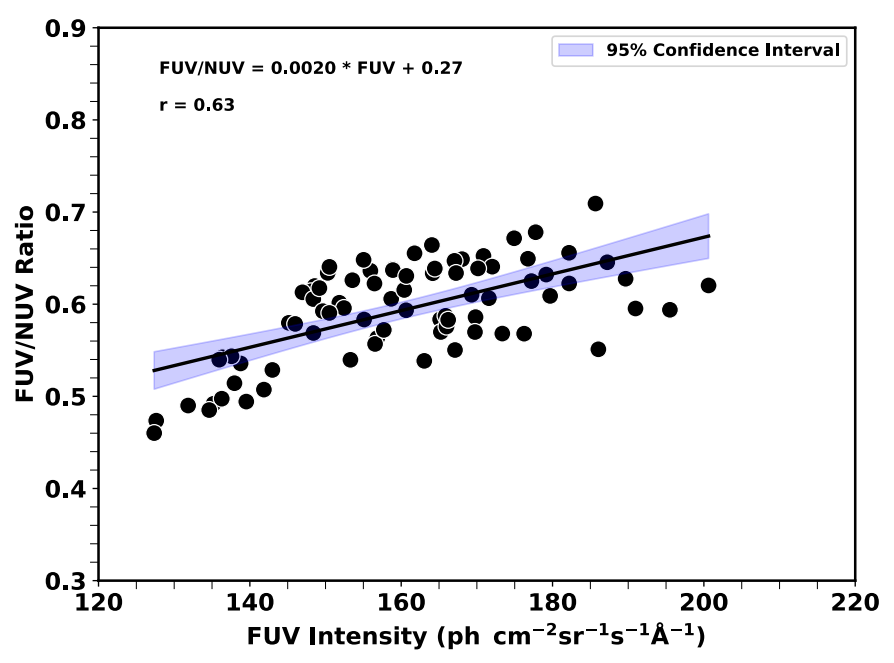


Figure 3. FUV/NUV intensity ratio plotted against FUV intensity, showing a moderate positive correlation (r = 0.63). The linear fit with a 95% confidence interval (shaded) indicates that regions with higher FUV intensities tend to exhibit enhanced FUV dominance with a reduced NUV contribution.

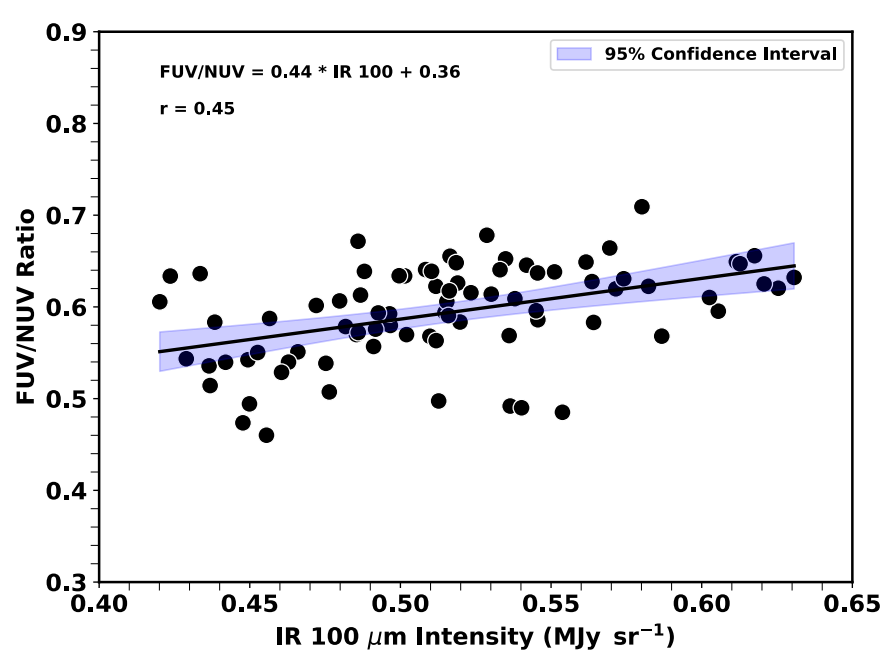


Figure 4. Variation of FUV/NUV intensity ratio as a function of $IR_{100} \mu m$ intensity, showing a moderate correlation (r = 0.45). Linear fit along with 95% confidence interval (shaded) is also shown.

constant for $|{\rm gb}| < 71^{\circ}.29$, but exhibits a clear variation above this limit in the region. Limiting the analysis to high latitudes ($|{\rm gb}| > 71^{\circ}.29$), the intensities of FUV and NUV are very closely related (Figure 7: r=0.85, NUV = 1.51 FUV + 21). The FUV-IR₁₀₀ correlation (Figure 8) stays the same at a moderate level of 50% (FUV = 147.63 IR₁₀₀ + 89), but NUV exhibits a weaker even

though improved dependency on IR_{100} compared to lower latitudes, with r=0.27 (NUV = 140.77 IR_{100} + 199). In conclusion, the results show that the FUV and NUV intensities track each other closely and the dust emission correlates more strongly with the FUV background than with NUV, especially at high Galactic latitudes. Diverse sensitivity to local radiation fields

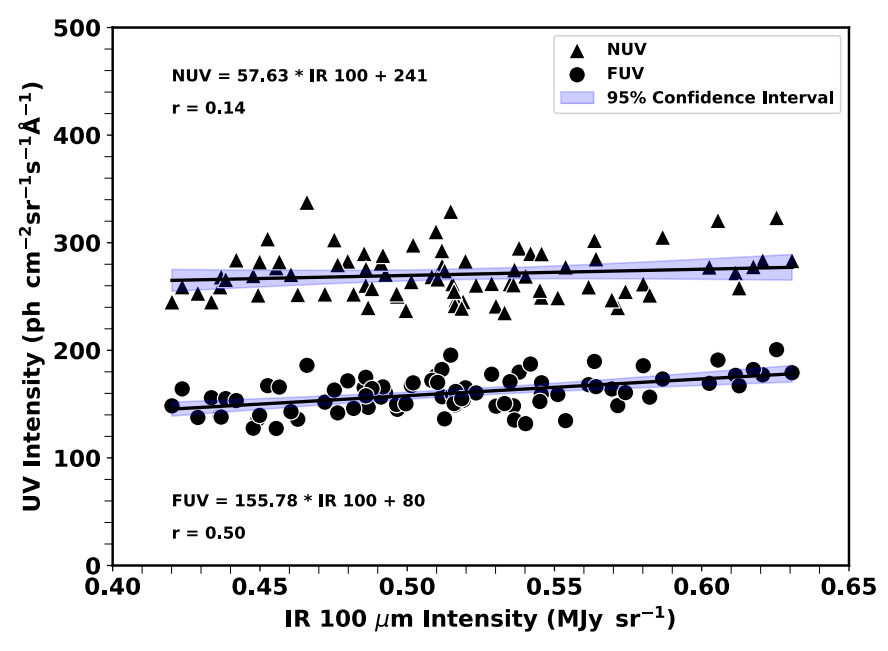


Figure 5. Correlation of UV intensities with IR₁₀₀ μ m emission in the PHOENIX_00 region. FUV (circles) shows a moderate correlation with IR₁₀₀ (r = 0.50), while NUV (triangles) exhibits a weaker correlation (r = 0.14). Linear fits with 95% confidence intervals (shaded) are shown, suggesting stronger dust-associated influence on FUV than NUV intensities.

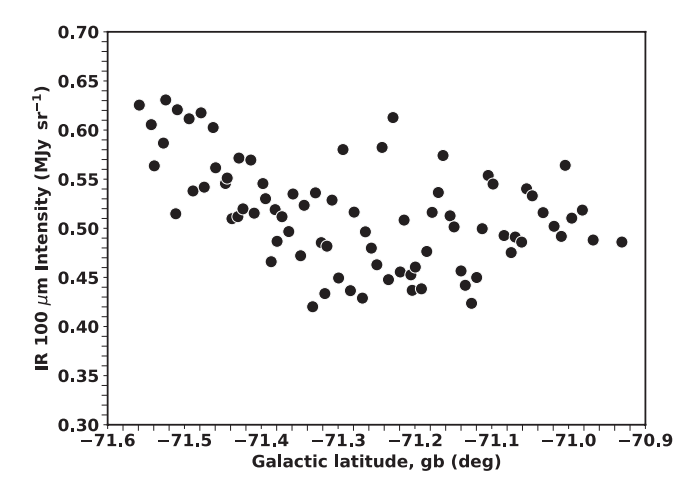


Figure 6. Variation of IR₁₀₀ μ m intensity with Galactic latitudes.

or supplementary NUV components unrelated to dust scattering may explain this discrepancy.

The diffuse UV emission in space is influenced by the ISRF, the presence of dust along the line of sight, and how dust grains scatter light. Using the model developed by Sujatha et al. (2004), we estimated the ISRF in our line of sight at 130 pc. In this model, the distance and spectral type of each star were taken from Hipparcos data (Perryman et al. 1997), and the flux was calculated using Kurucz models (Kurucz 1992), from his website (http://kurucz.harvard.edu). Even though the ISRF variation is not that prominent in the region, IR₁₀₀ micron emission shows an inverse correlation with the ISRF in both the UV bands (Figures 9 and 10) which is also reflected in the ISRF–FUV plot

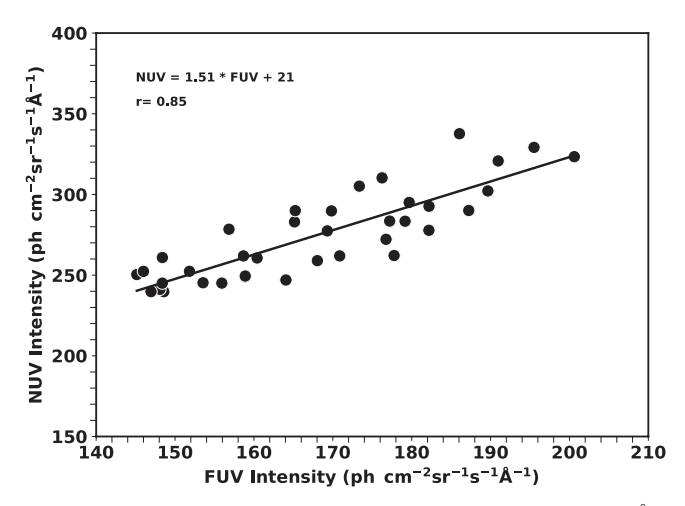


Figure 7. Correlation between FUV and NUV intensities for |gb| > 71.29.

(Figure 11). The negative correlation between ISRF and UV flux is likely due to dust absorption and the geometry of dust grains. We have modeled the scattered light to understand the underlying mechanisms driving the observed correlations.

The spread in the 95% confidence intervals of the linear fits in correlation plots of UV and IR intensities shows that the NUV scatters more than the FUV, suggesting that the FUV background is more reliably linked to thermal dust emission, while NUV intensities are influenced by additional, possibly uncorrelated factors. This difference highlights the complexity in interpreting NUV background sources and the relatively clearer dust-scattering contribution in the FUV band.

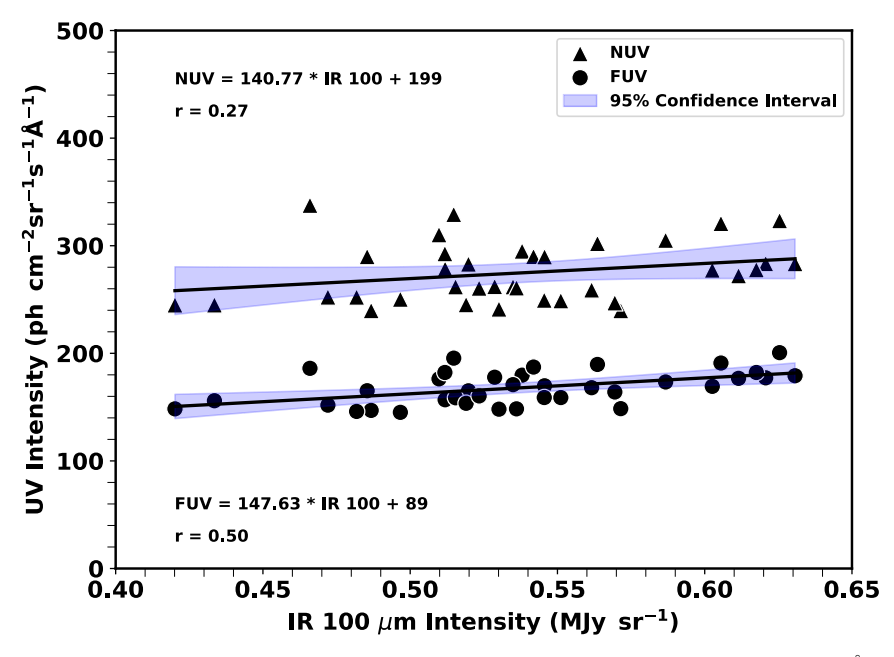


Figure 8. UV background intensities (FUV and NUV) plotted against IR₁₀₀ μ m intensity for high Galactic latitudes, |gb| > 71.29. The FUV intensities (circles) show a moderate correlation with IR₁₀₀ (r = 0.50), while the NUV intensities (triangles) exhibit a weaker correlation (r = 0.27). Linear fits with 95% confidence intervals are shown, suggesting varying degrees of dust-related influence on the UV intensities.

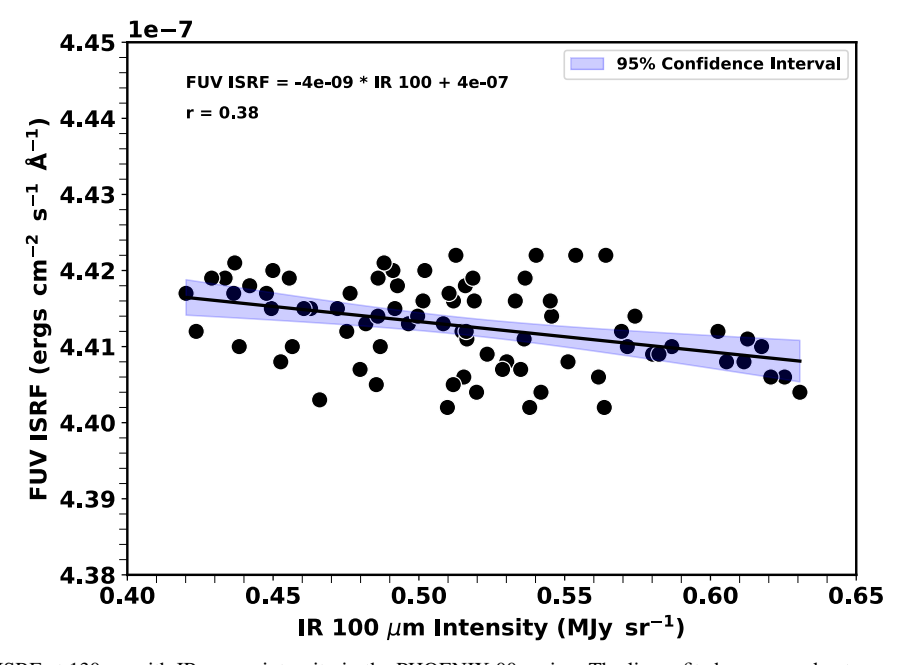


Figure 9. Variation of FUV ISRF at 130 pc with IR₁₀₀ μ m intensity in the PHOENIX 00 region. The linear fit shows a moderate negative correlation (r = -0.38), suggesting minimal dependence of the FUV ISRF on dust thermal emission.

The optical depth around the PHOENIX_00 target is very low and ranges between 0.09 and 0.15. So, a single scattering model can sufficiently explain the dust-scattered light in the region. We used the three-parameter model (albedo (a), phase function asymmetry factor (g) and distance of the cloud (d)) of interstellar dust scattering, as described in Sujatha et al.

(2005), to determine the optical constants of interstellar grains in the region. In this model, we use data from the Hipparcos Star catalog (Perryman et al. 1997) and Kurucz models (Kurucz 1992) to predict the radiation environment where dust scattering occurs. The scattered radiation from interstellar dust depends on the scattering function described by Henyey &

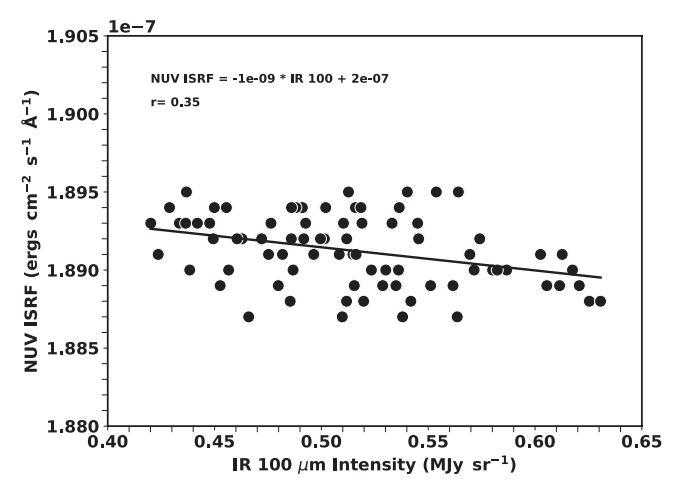


Figure 10. NUV ISRF at 130 pc plotted against $IR_{100} \mu m$ intensity.

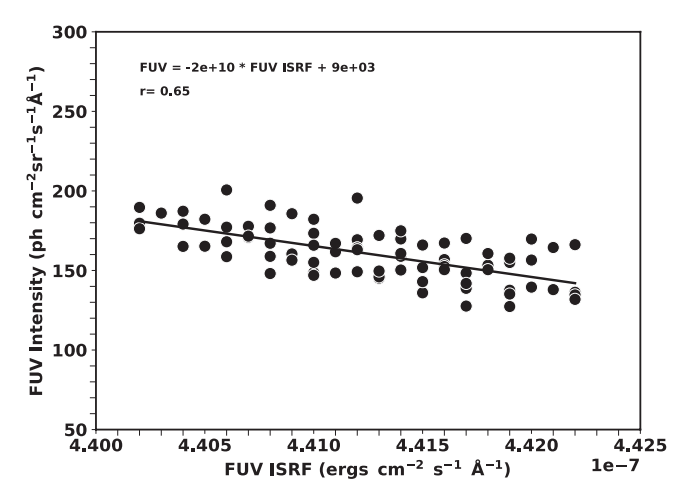


Figure 11. Variation of FUV intensity against FUV ISRF.

Greenstein (1941), which is a function of the grain albedo (a) and the phase function asymmetry factor (g). We observe a standard deviation of 16 PU in the FUV and 22 PU in the NUV bands for a 4' resolution. To accommodate for data scatter and foreground subtraction errors in chi-square minimization, we used 30 and 35 PU in FUV and NUV intensities as uncertainties. The a-g contour plots in Figures 12 and 13 show that a set of suitable a and g combinations can explain the observed UV intensities. The neutral hydrogen column density shows a moderate positive relationship with FUV and NUV radiation, as illustrated in Figures 14 and 15.

In the far-infrared (far-IR), dust emission mainly comes from large graphite and silicate grains (Désert et al. 1990; Dwek et al. 1997). However, in the mid-IR, the emission is mostly dominated by very small grains (PAHs). To better understand the nature of interstellar dust, we analyzed the four intensities of the IRAS band (12, 25, 60, and 100 μ m) and their ratios as a function of the 100 μ m surface brightness, IR₁₀₀, over the PHOENIX_00 region. Our study did not find a

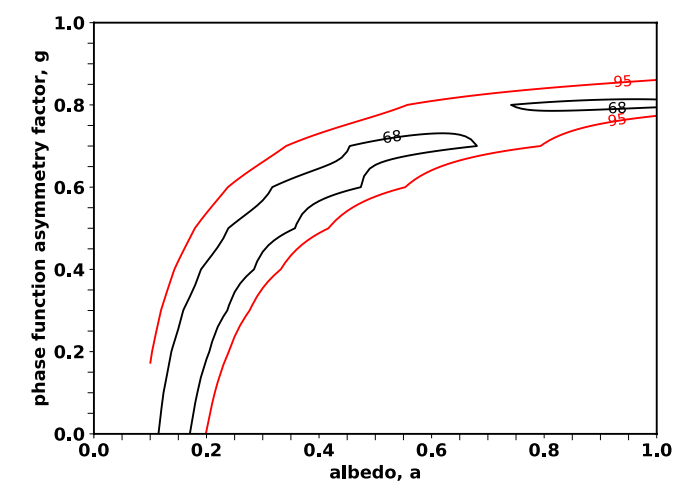


Figure 12. 1σ (68%, black) and 2σ (95%, red) confidence contours for the optical constants in FUV.

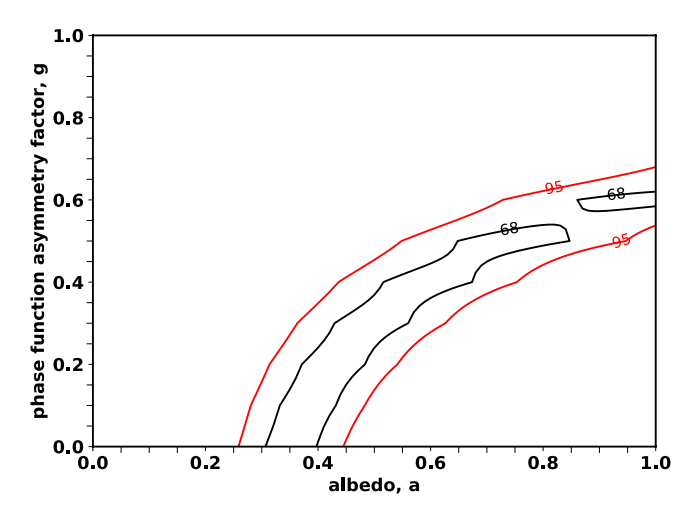


Figure 13. 1σ (black) and 2σ (red) confidence contours for the optical constants in NUV.

significant correlation between IR intensities at 12, 25, 60, 90, 140, and 160 μ m in this region. However, 60 and 100 μ m IR intensities, which represent warmer and cooler dust, respectively, are strongly correlated (r=0.8, IR₆₀ = 0.36 IR₁₀₀ + -0.03) in the region (Figure 16), indicating that both bands trace the same population of "big" dust grains heated by the general ISRF. This also implies that the temperature variations in dust in the regions are fairly uniform.

By analyzing intensity ratios in different IR bands, we can determine the type of dust that contributes to diffuse emission. We have seen that the IR 60–100 μm ratio is more or less constant at about 0.34 ± 0.03 in the region (Figure 17), indicating a nearly uniform equilibrium temperature of the large-grain population across the medium. The intensity ratio of IR 60–25 μm (IR $_{60}$ /IR $_{25}$) is often used as an indicator of hot dust (Wu et al. 2011). Studies by Tommasin et al. (2008, 2010) and Ramos Padilla et al. (2020) suggest that IR $_{60}$ /IR $_{25}$ ratios

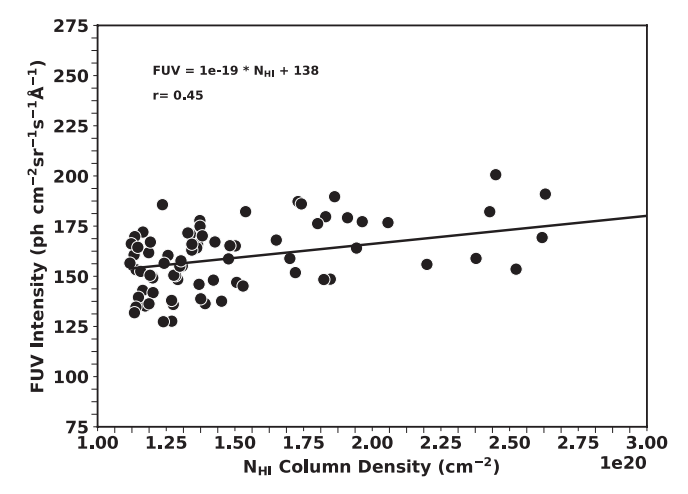


Figure 14. Correlation between FUV intensity and neutral hydrogen column density.

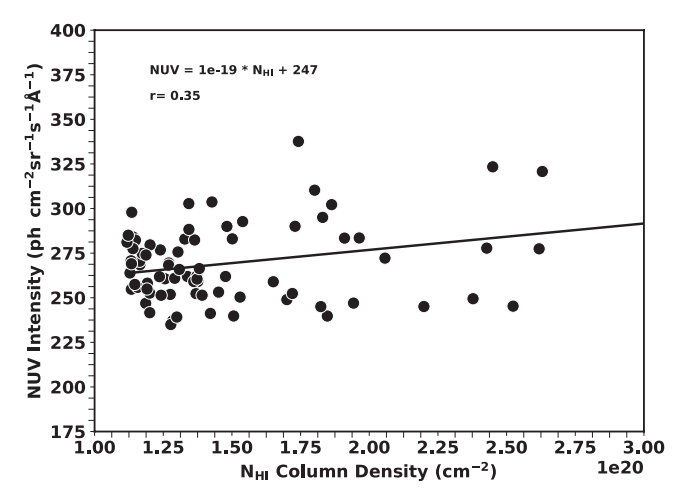


Figure 15. Correlation between NUV intensity and neutral hydrogen column density.

below 3 are typically associated with AGN-dominated systems, whereas ratios above 3 are more common in starforming galaxies. In our region, the IR₆₀/IR₂₅ ratio is less than 3, indicating that AGN activity is likely dominant in the region and that hot dust is relatively weak in the selected area. Furthermore, we observe a strong negative correlation between the IR_{12}/IR_{100} ratio and IR_{100} (Figure 18, r = 0.85, with a slope of -0.40), suggesting that as the far-IR brightness increases, the relative contribution of the very smallest grains (PAHs, which dominate at $12 \mu m$) drops, indicating either their destruction/coagulation in denser regions or increased self-shielding of the UV photons that excite them. Similarly, we also observed a stronger correlation with a steeper decline of IR_{25}/IR_{100} ratio (Figure 19), r = 0.97, with a slope of -0.81, with increasing IR₁₀₀, indicating that the very small grains responsible for the 25 μ m emission are highly depleted or heated less efficiently in the brightest (and presumably

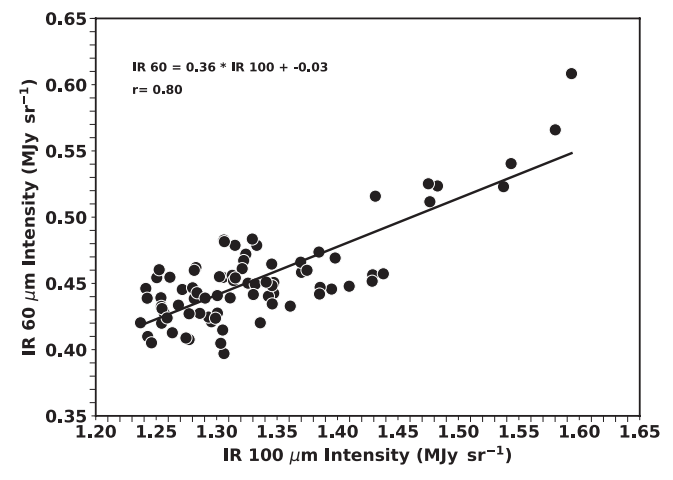


Figure 16. Correlation between $IR_{60} \mu m$ intensity and $IR_{100} \mu m$ intensity.

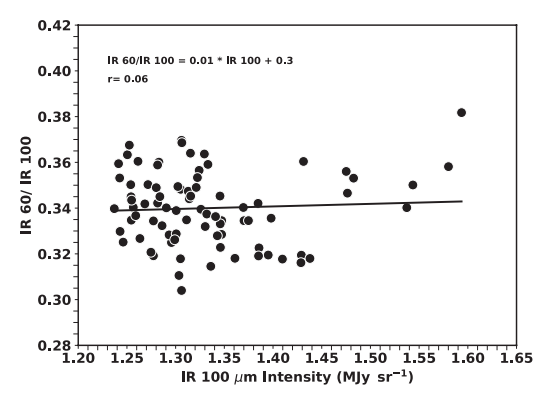


Figure 17. Ratio of IR₆₀ to IR₁₀₀ μ m intensities is plotted against IR₁₀₀ μ m.

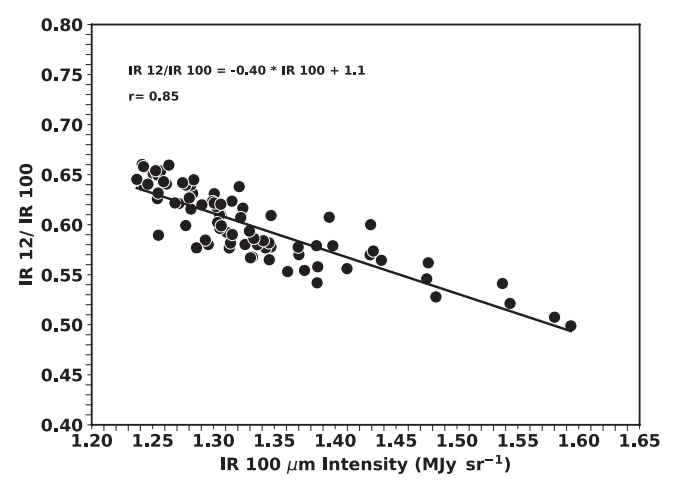


Figure 18. Ratio of IR₁₂ μ m and IR₁₀₀ μ m intensities is plotted against IR₁₀₀.

densest) regions. In short, we can say that stronger negative correlations of IR_{12}/IR_{100} ratio and IR_{25}/IR_{100} ratio with IR_{100} along with a moderate positive correlation (r=0.45) between the FUV/NUV ratio and IR_{100} (Figure 4) collectively indicate

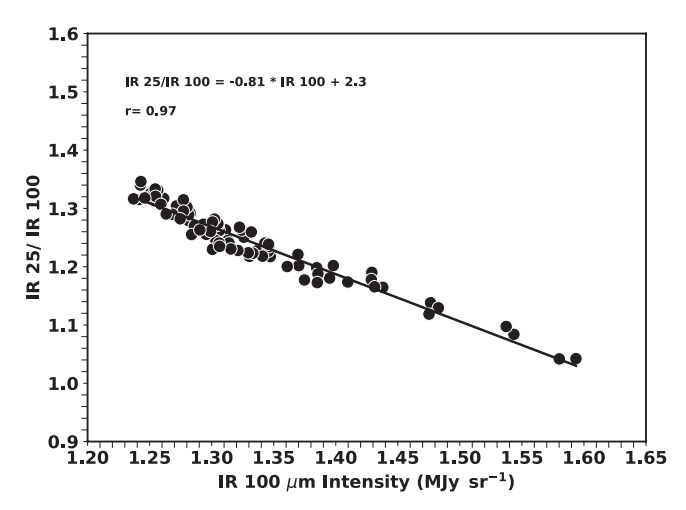


Figure 19. Variation of $IR_{25} \mu m$ to $IR_{100} \mu m$ intensity ratio against IR_{100} .

an environmental transition in dust characteristics: regions with higher IR_{100} intensities exhibit a transition from smaller, warmer grains to larger, cooler grains, accompanied by minor changes in the UV scattering efficiency-possibly indicating enhanced FUV dominance due to dust evolution or depletion of NUV-absorbing components such as PAHs.

To identify the source of the significant amount of nonzero intercept in the IR₁₀₀-UV plots, we calculated the contribution of EGL, whose dominant sources are galaxies and AGNs (Upton Sanderbeck et al. 2018). We estimated EGL using point sourceremoved FITS files of diffuse UV background. The positions of galaxies and AGNs within a 0.55 radius of the PHOENIX 00 target were obtained from the SIMBAD database (Wenger et al. 2000) and the WISE AGN catalog (Assef et al. 2018). The EGL contribution of each source was calculated considering the flux within a 5 pixel (7.5) annular ring surrounding each source. The sum of the flux contributions from each source was used to obtain the overall EGL. We evaluated the error in the EGL computation using annular rings of 4 pixels (6") and 6 pixels (9"). The EGL contribution from galaxies and AGNs was found to be 4 \pm 2 PU and 6 \pm 4 PU in the FUV and 18 \pm 11 and 27 \pm 18 PU in the NUV, respectively. In the diffuse UV background, the overall EGL contribution was 45 \pm 29 PU in NUV and 10 \pm 6 PU in FUV. Our result is in good agreement with Welch et al. (2020) in the FUV. By comparing the estimated EGL values with the nonzero intercept of IR₁₀₀-UV plots, we discovered that 10 ± 6 of the 89 ± 16 PU in FUV are EGL, while 45 ± 29 of the 199 \pm 22 PU in NUV are EGL.

4. Conclusion

We investigated the PHOENIX_00 region close to galaxy clusters in UV using GALEX deep observations and detected a diffuse background of about 160 ± 16 PU in the FUV band and 270 ± 22 PU in the NUV band in addition to the foreground emissions. There is a moderate correlation between the FUV

and NUV intensities in the region, with NUV scaling positively with FUV. At higher FUV intensities, FUV emission prevails over NUV emission, as evidenced by a stronger correlation between FUV and the FUV/NUV ratio (r=0.63). Overall, our findings highlight the significant influence of FUV emissions in studying dust properties, while NUV behavior appears more complex and possibly affected by other sources such as relatively faint sources which have negligible effects in the FUV. However, the FUV/NUV ratio is less than unity, suggesting that there are no extra contributions from other sources, such as hot line emissions or H_2 fluorescence.

Our analysis reveals a moderate correlation between FUV intensity and IR₁₀₀ emissions, indicating that dust-related activities have a significant impact on the FUV background radiation. NUV intensities, on the other hand, show far weaker correlations, most likely because of their decreased sensitivity to dust fluctuations, as seen by the significant scatter in GALEX data. At high Galactic latitudes ($|gb| > 71^{\circ}.29$), both UV bands exhibit stronger intercorrelation, emphasizing their mutual consistency in areas with low dust density. However, even at these latitudes, the relationship between IR₁₀₀ and FUV is still moderate and weaker for NUV, reaffirming that dust emissions predominantly affect the FUV regime. Collectively, these findings highlight the critical role dust plays in modulating the FUV background relative to the NUV, particularly at higher Galactic latitudes, providing valuable insights into the complex interplay between UV radiation and interstellar dust.

Furthermore, for both UV bands, we found an inverse relationship between IR $_{100}$ emissions and ISRF. By investigating the relationships between UV and IR emissions at various wavelengths (12, 25, 60, and $100\,\mu\text{m}$), we discovered that small-grain/PAH emission (12 and 25 μm), when normalized to $100\,\mu\text{m}$, sharply declines in brighter (denser) regions, while biggrain emission (60 and $100\,\mu\text{m}$) scales together and maintains a roughly constant color temperature. A depletion or reduced excitation of smaller grains in places of higher column density-likely due to coagulation into larger aggregates and/or UV-shielding effects-and a reasonably uniform heating of the large-grain component by the ISRF are consistent with this trend.

Our analysis of IR intensity ratios has shed important light on the dust properties of the area under study. While an observed IR_{60}/IR_{25} ratio less than 3 indicates domination by an AGN and relatively modest emission from hot dust, the consistent IR_{60}/IR_{100} ratio $(\approx\!0.34\pm0.03)$ shows a uniform equilibrium temperature among big dust grains. Significant depletion or decreased excitation efficiency of very small grains and PAHs within denser, brighter regions is indicated by the markedly negative correlations of IR_{12}/IR_{100} and IR_{25}/IR_{100} ratios with increasing IR_{100} brightness. This is most likely caused by grain destruction, coagulation, or increased self-shielding from UV photons.

The nonzero intercept in IR_{100} –UV intensity plots is influenced by EGL in the region, which accounts for approximately 10 ± 6 PU (11%) of the 89 ± 16 in diffuse FUV and 45 ± 29 PU (23%) of the 199 ± 22 in diffuse NUV, also has some impact on the nonzero intercept displayed in IR_{100} –UV intensity plots. Our three-parameter model of dust-scattered radiation explains the remaining radiation as starlight with varying optical constants in the region. These findings show the complex interactions between dust composition, ambient density, radiation fields, and extragalactic contributions in determining IR and UV emissions in interstellar regions.

Acknowledgments

SNV, MKM & FKF acknowledge the support and facility of DST-FIST @ SXC. This study is based on GALEX data from NASA. The data reported in this research were gathered from the Mikulski Archive for Space Telescopes (MAST) (https://galex. stsci.edu/GR6/). We have also used NASA's Astrophysics Data System (https://ui.adsabs.harvard.edu/) for literature survey. We recognize the usage of NASA's SkyView facility (https:// skyview.gsfc.nasa.gov) at NASA Goddard Space Flight Center. This research has made use of the SIMBAD database (http:// simbad.cds.unistra.fr/simbad/, operated at CDS, Strasbourg, France. For data analysis, the programming languages Gnu Data Language (https://gnudatalanguage.sourceforge.net/index.php) and Python modules including Astropy, NumPy, and SciPy were used. We thank the anonymous referee for the valuable suggestions that helped us clarify several aspects of the article. Facility: GALEX.

ORCID iDs

N. V. Sujatha https://orcid.org/0000-0001-6787-6080

References

Assef, R. J., Stern, D., Noirot, G., et al. 2018, ApJS, 234, 23 Bertin, E., & Arnouts, S. 1996, A&AS, 117, 393

```
Bohlin, R. C., Savage, B. D., & Drake, J. F. 1978, ApJ, 224, 132
Bordoloi, O. P., Ananthamoorthy, B., Shalima, P., et al. 2024, PASP, 136,
Bowyer, S. 1991, ARA&A, 29, 59
Burchett, J., Butsky, I., Tremmel, M., et al. 2019, BAAS, 51, 534
Cox, D. P. 2005, ARA&A, 43, 337
Draine, B. T. 2003, ARA&A, 41, 241
Dwek, E., Arendt, R. G., Fixsen, D. J., et al. 1997, ApJ, 475, 565
Désert, F. X., Boulanger, F., & Puget, J. L. 1990, A&A, 237, 215
Finkbeiner, D. P. 2003, ApJS, 146, 407
Gil de Paz, A., Boissier, S., Madore, B. F., et al. 2007, ApJS, 173, 185
Hamden, E. T., Schiminovich, D., & Seibert, M. 2013, ApJ, 779, 180
Henry, R. C. 1991, ARA&A, 29, 89
Henyey, L. G., & Greenstein, J. L. 1941, ApJ, 93, 70
HI4PI Collaboration, Ben Bekhti, N., Flöer, L., et al. 2016, A&A, 594, A116
Kurucz, R. L. 1992, in IAU Symp., The Stellar Populations of Galaxies, 149,
  ed. B. Barbuy & A. Renzini (Dordrecht: Kluwer), 225
Leinert, C., Bowyer, S., Haikala, L. K., et al. 1998, A&AS, 127, 1
Martin, D. C., Fanson, J., Schiminovich, D., et al. 2005, ApJL, 619, L1
Miville-Deschênes, M.-A., & Lagache, G. 2005, ApJS, 157, 302
Morrissey, P., Conrow, T., Barlow, T. A., et al. 2007, ApJS, 173, 682
Murakami, H., Baba, H., Barthel, P., et al. 2007, PASJ, 59, S369
Murthy, J. 2016, MNRAS, 459, 1710
Murthy, J., Henry, R. C., & Sujatha, N. V. 2010, ApJ, 724, 1389
Narayanan, N., Menon, S. S., & Sujatha, N. V. 2023a, AdSpR, 71, 1059
Narayanan, N., Menon, S. S., & Sujatha, N. V. 2023b, RAA, 23, 065021
Perryman, M. A. C., Lindegren, L., Kovalevsky, J., et al. 1997, A&A,
  323, L49
Planck Collaboration, Abergel, A., Ade, P. A. R., et al. 2014, A&A, 571, A11
Ramos Padilla, A. F., Ashby, M. L. N., Smith, H. A., et al. 2020, MNRAS,
  499, 4325
Schlegel, D. J., Finkbeiner, D. P., & Davis, M. 1998, ApJ, 500, 525
Sujatha, N. V., Chakraborty, P., Murthy, J., & Henry, R. C. 2004, BASI,
Sujatha, N. V., Murthy, J., Karnataki, A., Henry, R. C., & Bianchi, L. 2009,
   ApJ, 692, 1333
Sujatha, N. V., Murthy, J., Suresh, R., Conn Henry, R., & Bianchi, L. 2010,
   ApJ, 723, 1549
Sujatha, N. V., Shalima, P., Murthy, J., & Henry, R. C. 2005, ApJ, 633, 257
Tommasin, S., Spinoglio, L., Malkan, M. A., & Fazio, G. 2010, ApJ,
  709, 1257
Tommasin, S., Spinoglio, L., Malkan, M. A., et al. 2008, ApJ, 676, 836
Upton Sanderbeck, P. R., McQuinn, M., D'Aloisio, A., & Werk, J. K. 2018,
   ApJ, 869, 159
Welch, B., McCandliss, S., & Coe, D. 2020, AJ, 159, 269
Wells, D. C., Greisen, E. W., & Harten, R. H. 1981, A&AS, 44, 363
Wenger, M., Ochsenbein, F., Egret, D., et al. 2000, A&AS, 143, 9
Wu, Y.-Z., Zhao, Y.-H., & Meng, X.-M. 2011, ApJS, 195, 17
Zhitnitsky, A. 2022, PhLB, 828, 137015
```